2022

Battery Cooling Module Optimization Method: Battery Lifetime Prediction Using Temperature

Se Hyeon Ham

Dong Soo Jang

Yongchan Kim

Optimization Method of Battery Cooling Module: Battery Lifetime Prediction using Temperature

Se Hyeon Ham[1], Dong Soo Jang[2], Yongchan Kim[3*]

[1]Graduate School of Mechanical Engineering, Korea University, Anam-ro 145, Seongbuk-gu, Seoul, Korea
un2179@korea.ac.kr

[2]Engineering Laboratory, National Institute of Standards and Technology, Gaithersburg, MD 20899, USA
nicebb0y7@korea.ac.kr

[3]Department of Mechanical Engineering, Korea University, Anam-ro 145, Seongbuk-gu, Seoul, Korea
yongckim@korea.ac.kr

* Corresponding Author

ABSTRACT

With the growth of the renewable energy and electric vehicle market, the battery market is growing significantly. Lithium-ion batteries have many advantages such as longevity and specific output. However, lifespan, capacity, and stability of the lithium-ion batteries are greatly affected by its temperature and temperature gradient. In addition, a battery itself generates heat when in use. Accordingly, a battery must be stored and used at an optimum temperature. Therefore, an effective battery thermal management system (BTMS) is to be developed to improve battery performance. The objective of this study is to predict the lifetime of the pouch type NMC battery according to the performance of the battery cooling module. In the cooling module, the cooling performance varies with respect to the cooling method and shape, and the performance may also vary significantly. To quantitatively compare the difference in cooling performance, the temperature and its gradient on the battery surface were converted into cooling performance parameter (CPP) and equivalent full cycle (EFC). The performance of the cooling module presented in previous studies was compared in terms of CPP and EFC. Finally, the design parameters were optimized to improve the lifespan of the pouch-type lithium-ion batteries.

1. INTRODUCTION

As interest in new and renewable energy is growing, the market for energy storage devices is expanding. One of the most important goals for electric vehicles is to improve power output and driving range. To achieve these goals, lithium-ion batteries are widely used in electric vehicles because they have higher specific power, specific capacity and longer lifespan compared to other energy storage devices. Although lithium-ion batteries have many advantages, they have a problem of high sensitivity to temperature.

To ensure operating characteristics such as safety, performance, capacity, and lifespan, lithium-ion batteries must be used within an appropriate operating temperature and temperature distribution inside the battery cell (Feng et al., 2018). When the environmental temperature is low, such as in winter, the chemical reaction slows down and the capacity decreases, whereas, in high temperature such as summer, the lifespan is shortened and the possibility of thermal runaway increases (Wilke et al., 2017). It was shown that the lifespan of NMC532 type lithium-ion battery was reduced by 30% and 50% at 10 ℃ and 40 ℃, respectively, compared to that at 25 ℃ (Xu et al., 2019). In addition, not only heat exchange with the outside through boundaries but also heat generated by itself occur during the use of the battery. Therefore, to ensure effective use and safety, the battery must be maintained at an appropriate

temperature (Wang et al., 2016), and the temperature distribution in the battery module must be kept small (Pesaran, 2002).

In the battery pack, various cooling systems have been applied to maintain the battery's temperature constant. An air-cooling system for the battery pack has been widely used in early commercial electric vehicles, but it shows poor heat transfer performance. A liquid-cooling system has a disadvantage of complicated design with heavy weight compared to other cooling methods. However, most commercial electric vehicles adopt the liquid-cooling method owing to its high heat transfer performance and effective temperature control capability.

The optimization of cooling modules has been extensively studied. Many researchers have investigated various methods such as metal fins, water jackets, and direct cooling to improve cooling performance. Furthermore, not only cooling methods but also design and operating condition optimizations have been carried out. However, study on lifespan prediction of battery cooling was hardly carried out. In the viewpoint of system optimization, Jarret and Kim (2011) noted that the optimal shape of the battery cooling module can vary depending on the target parameter.

In this study, the optimization of the battery pack was conducted by using an equivalent full cycle (EFC). The EFC is a parameter of the aging temperature, which indicates an aging rate of the battery. The performance of the cooling module under various conditions was evaluated by numerical analysis to compare the conventional parameter with EFC. As a result, the optimized design parameters were proposed for the prediction of battery lifespan.

2. Method

Figures 1(a) and (b) show the geometry and transparent view used in CFD, respectively. The cooling module consists of six high-performance pouch-type batteries and seven cooling fins. A flow path was designed inside the fins to have coolant flow, and the fins were installed between the batteries. Heat from the battery transferred through the fins and coolant.

Figure 1(c) shows three specific areas in the battery cell. The calculation domain was divided into the cathode area (area 1), anode area (area 2), and bottom area (area 3) to reflect the uneven and time-variant heat generation in the battery cell. The heat generation in a battery consists of irreversible and reversible heat generations, as shown in Equation (1). Irreversible heat is mainly ohmic heat generated by the flow of current, and reversible heat is generated by entropy change from chemical reaction. Therefore, it can be assumed that irreversible heat in a battery is proportional to the square of the current, and reversible heat is proportional to the current. During the discharge process, although irreversible heat generation does not vary, reversible heat generation changes significantly depending on the stage of charge. In addition, even if the current is uniformly generated in the battery, the current is passing through the battery tab. Thus, non-uniform and time-variant heat generation occurs in a battery.

$$Q_{total} = Q_{rev} + Q_{irrev} \tag{1}$$

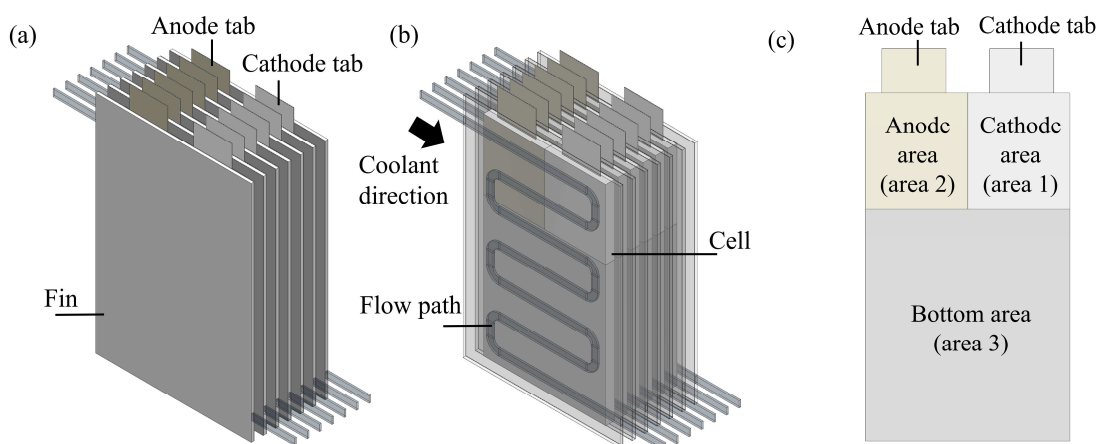$$Q(x)_{area.n} = A_0 + A_1 x + A_2 x^2 + A_3 x^3 + A_4 x^4 \tag{2}$$

Figure 1: (a) Battery module assembly, (b) assembly transparent view, and (c) battery cell and three areas.

In this study, a numerical analysis on the battery cell was conducted when the fully charged battery was completely discharged at 5C discharge. The non-uniform and time-variant heat generation in the battery was predicted by calculating the heat value using a polynomial correlation, as given in Equation (2). Table 1 shows the coefficients, which were obtained through an experiment of discharging the battery. The battery was a 40 Ah pouch-type lithium-ion cell with an NMC532 cathode and graphite anode. Figure 2 shows the calculated heat generation value for each area.

Table 1: Coefficients of the battery heat generation correlations.

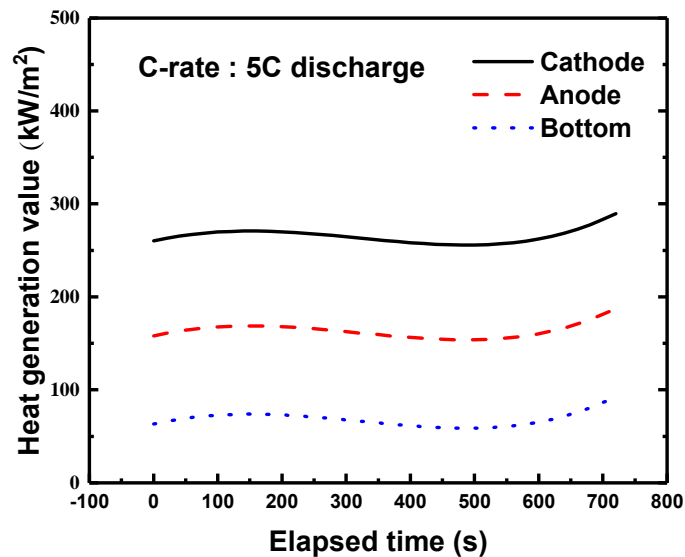| Area 1 Parameter	Value	Area 2 Parameter	Value	Area 3 Parameter	Value
A_0	2.6051E2	A_0	1.5802E2	A_0	6.3805E1
A_1	1.1223E2	A_1	1.1223E2	A_1	1.1223E2
A_2	-3.3989E2	A_2	-3.3989E2	A_2	-3.3989E2
A_3	2.1398E2	A_3	2.1398E2	A_3	2.1398E2
A_4	4.3186E1	A_4	4.3186E1	A_4	4.3186E1

Figure 2: Heat generation value for each area.

The cooling path was varied according to its shape and flow arrangement. Figure 3 shows the shapes of three types of cooling paths for the fins used in this study: simple serpentine, symmetry serpentine, and double serpentine. The simple serpentine, symmetry serpentine, and double serpentine are called paths A, B, and C, respectively. Two arrangements were used in this study: the anode side and cathode side arrangements. In the anode side arrangement, the coolant passes the anode area first, whereas, in the cathode side arrangement, the coolant passes the cathode area first.

Specifications of poly-hexagonal mesh used in this study were as follows: the number of cells and faces was 10–30 million; the maximum inverse orthogonal quality was less than 0.85; K-omega SST turbulence model was used, and the average y+ was 2.1–2.2.

Table 2 lists the simulation conditions. The inlet velocity in the cooling paths was set to 0.5 m/s, and the total flow rates through the fins were the same. The coolant temperature was set to 26.8 ˚C (300 K). Water was used as the

coolant. All wall boundaries were set to adiabatic condition. The amount of heat generated by the current flowing through the busbar was omitted based on the assumption that the generated heat and transferred heat outside were the same.
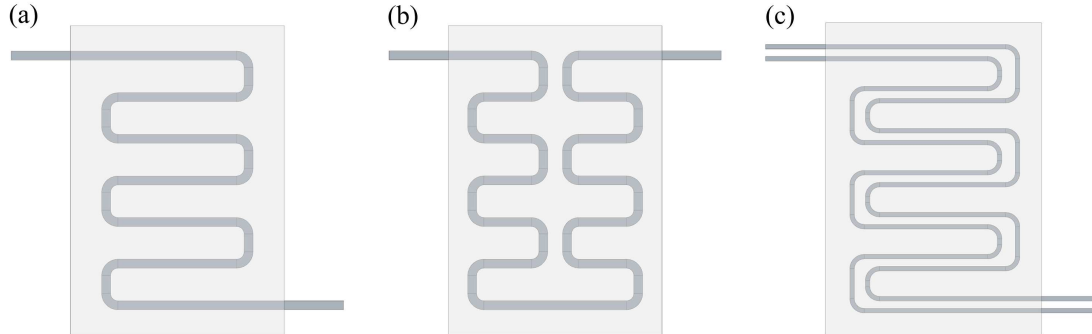

Figure 3: Geometries of cooling paths: (a) simple serpentine flow path, (b) symmetry serpentine flow path, and (c) double serpentine flow path.

Table 2: Analysis conditions for battery cooling module.

Parameter	Conditions
Cooling path arrangement	Anode side arrangement
	Cathode side arrangement
Cooling path type	Simple serpentine (path A)
	Symmetry serpentine (path B)
	Double serpentine (path C)

Normalized CPP ($P_{c.avg.normal}$) was calculated using the average temperature rise (ΔT_{avg}) between the starting and ending moments to evaluate the cooling performance of the battery module, as given in Equation (3). The lifespan was predicted using EFC, a novel method proposed in this study that uses the Arrhenius plot. As given in Equation (4), normalized EFC (EFC_{normal}) was calculated using the activation barrier (E_a), Boltzmann constant (K_b), and aging temperature (T_{aging}). The aging temperature was obtained using the average ($T_{average}$) and maximum difference ($T_{max.diff}$) of the temperature as given in Equation (5) (Fleckenstein, 2012).

$$P_{c.avg.normal} = \frac{\Delta T_{avg.base}}{\Delta T_{avg}} \tag{3}$$

$$EFC_{normal} = \frac{A\exp(-\frac{E_a}{K_B T_{aging.base}})}{A\exp(-\frac{E_a}{K_B T_{aging}})} \tag{4}$$

$$T_{aging} = T_{average} + 0.1 * T_{max.diff} \tag{5}$$

3. Results and Discussion

Figures 5 and 6 show the temperature contours according to the cooling path in the anode and cathode side arrangements, respectively. The highest temperature was observed near the tab owing to the current concentration,

whereas the lowest temperature was observed at the bottom side. This trend indicates that enhancing tab cooling can allow to have an effective cooling for the battery module. In addition, the cooling performance can be improved by optimizing the cooling paths for anode and cathode tabs owing to the difference in the heat generation between the anode and cathode tab sides.

Figure 7 shows the normalized CPP and EFC. The CPP and EFC for paths B and C were normalized based on the result for path A. In path C with the anode side arrangement, the normalized CPP and EFC were 1.087 and 1.052, respectively, owing to the excellent heat dissipation performance for path C with the coolant flowing in the opposite direction. The CPP and EFC were not varied according to the arrangement. In path B with the anode side arrangement, the normalized CPP and EFC were 1.031 and 0.988, respectively, the CPP was higher than that for path A owing to overall heat transfer performance improvement from the increased number of curves in the flow path. However, the EFC for path B was lower than that for path A owing to the increased temperature difference with the warmed coolant flow to the tab area. The CPPs for path B with the anode and cathode side arrangement were 1.031 and 1.087, respectively, and The EFCs were 0.9881 and 0.9898, respectively. The CPP for path B with the cathode side arrangement was higher than that in the anode side arrangement, whereas the EFC did not vary significantly with respect to the arrangement. This was because the average and difference in the temperature varied depending on the method. Thus, the optimization could be different depending on the objective parameter. In addition, the symmetric serpentine path is not a good option for lifespan improvement.
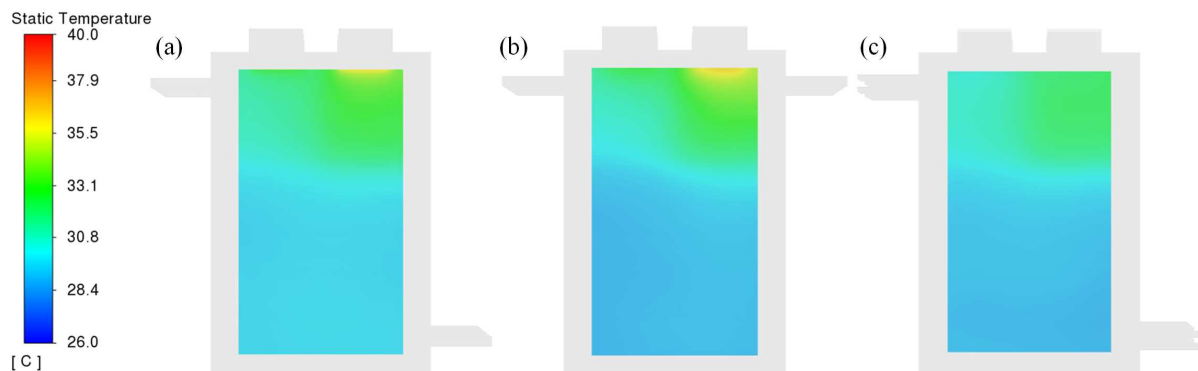

Figure 5: Temperature contours according to cooling path in anode side arrangement: (a) simple serpentine flow path, (b) symmetry serpentine flow path, and (c) double serpentine flow path.
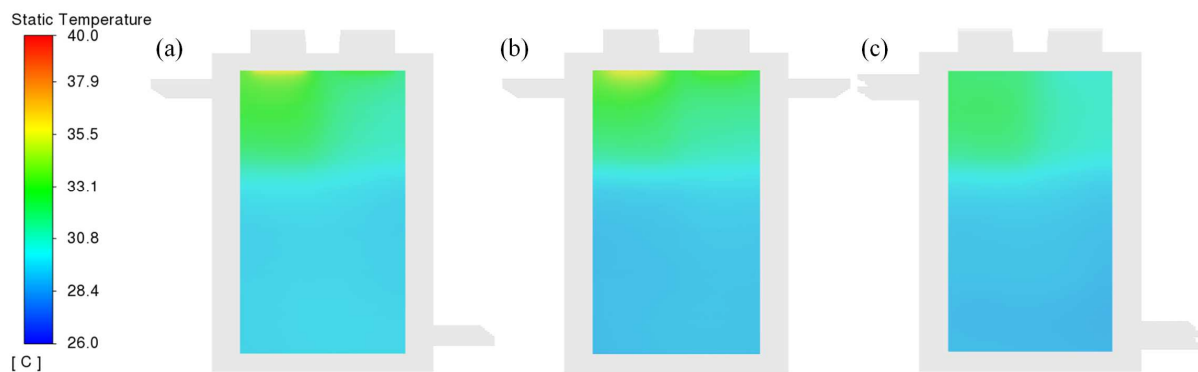

Figure 6: Temperature contours according to cooling path in cathode side arrangement: (a) simple serpentine flow path, (b) symmetry serpentine flow path, and (c) double serpentine flow path.
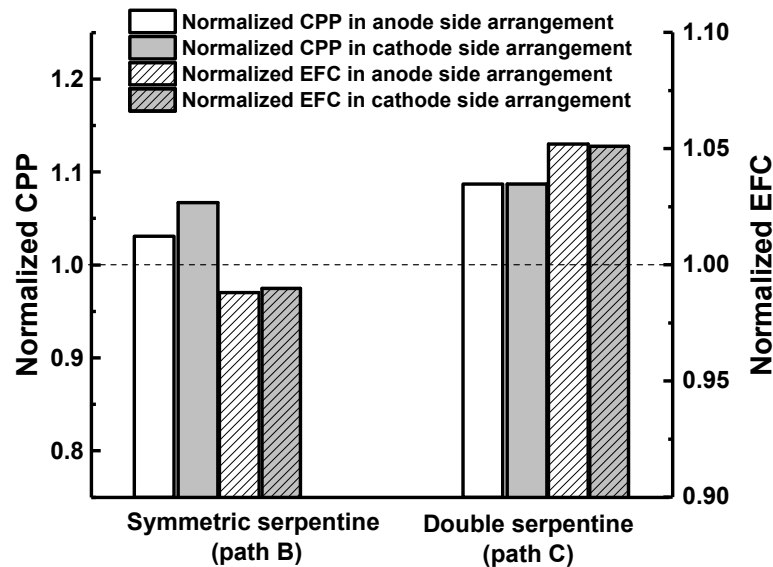
Figure 7: Normalized CPP and EFC for simple serpentine cases.

4. Conclusion

In this study, the thermal performance of the cooling modules was analyzed according to the cooling path design. A CFD analysis was conducted to estimate the performance of the cooling modules with different design specifications. As a result, in the symmetric serpentine flow path, the CPP increased 3.1-8.7%, whereas the EFC decreased 1.1-1.2%. In the double serpentine flow path, both the CPP and EFC increased 6.7-8.7% and 5.1-5.2%, respectively. In the cooling system arrangement, the cathode side arrangement was the optimal based on the CPP, but the anode side arrangement was the optimal based on the EFC. In conclusion, the optimal design varied with the objective parameter.

ACKNOWLEDGMENTS

NOMENCLATURE

A	pre-exponential factor	(°C)
CPP	cooling performance parameter	(W/°C)
E_a	activation barrier	(eV)
K_b	Boltzmann constant	(eV/°C)
$P_{c.avg.normal}$	normalized average CPP	(W/°C)
$Q_{area.n}$	local heating rate	(W/m³)
Q_{irrev}	irreversible heating rate	(W)
Q_{rev}	reversible heating rate	(W)
Q_{total}	total heating rate	(W)
T_{aging}	aging temperature	(°C)
$T_{max.diff}$	maximum temperature difference	(W)
ΔT_{avg}	average temperature rise	(°C)
$\Delta T_{avg.base}$	baseline average temperature rise	(°C)

Acronyms

CFD	computation fluid dynamic
EFC	equivalent full cycle
NMC	nickel manganese cobalt

REFERENCES

Feng, X., Ouyang, M., Liu, X., Xia, Y., He, X. (2018). Thermal runaway mechanism of lithium ion battery for electric vehicles: a review, Energy Storage Mater. 10, 246–267.

Fleckenstein, M., Bohlen, O., Baker, B. (2012). Aging effect of temperature gradients in Li-ion cells experimental and simulative investigations and the consequences on thermal battery management, World Electr. J. 5(2), 322–333.

Jarret, A., Kim, I. Y. (2011). Design optimization of electric vehicle battery cooling plates for thermal performance, J. Power Sources 196(23), 10359–10368.

Pesaran, A. A. (2002). Battery thermal models for hybrid vehicle simulations, J. Power Sources 110(2), 377–382.

Wang, Q., Jiang, B., Li, B., Yan, Y. (2016). A critical review of thermal management models and solutions of lithium-ion batteries for the development of pure electric vehicles, Renew. Sustain. Energy Rev. 64, 106–128.

Wilke, S., Schweitzer, B., Khateeb, S., Al-Hallaj, S. (2017). Preventing thermal runaway propagation in lithium in battery packs using a phase change composite material: an experimental study, J. Power Sources 340, 51–59.

Wu W., Wang, S., Wu, W., Chen, K., Hong, S., Lai, Y. (2019). A critical review of battery thermal performance and liquid based battery thermal management, Energy Convers. Manage. 182, 262–281.